Investigation of Ti/Au Transition-Edge Sensors for Single-Photon Detection

(Article begins on next page)

03 May 2024

Investigation of Ti/Au Transition-Edge Sensors for Single Photon Detection

Xiaolong Xu 1 • Mauro Rajteri 2 • Jinjin Li 1 • Shuo Zhang 3 •
Carlo Pepe 2,4 • Jian Chen 1 • Huifang Gao 1 • Qi Li 1 • Wei Li 1 •
Xu Li 1 • Mingyu Zhang 1 • Yanyan Ouyang 1 • Xueshen Wang 1

National Institute of Metrology (NIM), 100029 Beijing, China
Istituto Nazionale di Ricerca Metrologica (INRiM), 10135 Torino, Italy
ShanghaiTech University, 201210 Shanghai, China
Politecnico di Torino, 10129 Torino, Italy

Abstract Transition-edge sensors (TES) are remarkable superconducting devices for a wide range of radiation detection with the ability of both energy resolution and counting photons. For the detection of single photons at telecom wavelength, optical Ti/Au bilayer TESs are fabricated and characterized. The superconducting transition temperature (T_c) of the Ti/Au films are effectively tuned from 162 mK to 72 mK by increasing the relative thickness ratio between the Au and Ti layer. The sensitive area is 20 μm × 20 μm, on which an SiO_2/SiN_x antireflection structure is coated by an ICP-PECVD process. The TES device shows an energy resolution of 0.19 eV and can discriminate up to 36 incident photons, with an effective time constant around 107 μs at 95 mK.

1 Introduction

Superconducting transition-edge sensors (TESs) have been widely used for single photon detection from near infrared, visible light, X-ray to even γ-ray. The most distinctive feature of TESs is the single photon energy resolution and the photon-number resolving (PNR) capability (when the photon energy is already known) [1], but they also show high quantum efficiency [2], negligible dark counts [3] and show great potential in quantum information [4], dark matter detection [5], X-ray free-electron laser [6], satellite X-ray observatory [7] and cosmic microwave background observatory [8]. In the

Xiaolong Xu 1 • Mauro Rajteri 2 • Jinjin Li 1

1 field of optical metrology, TESs will realize the quantum revolution of
2 photometry [9].
3   In this paper we report about the fabrication and preliminary
4 characterization of optical Ti/Au TESs for single photon detection at telecom
5 wavelength. The critical temperature T_c of Ti/Au superconducting films is
6 tuned by controlling the thickness ratio of the two layers. An antireflection
7 SiO_2/SiN_x coating is deposited on the Ti/Au bilayer film before the
8 alignment of an optical fiber, and the simulated reflectivity is shown. The
9 TES device shows a high energy resolution (0.19 eV) and PNR capability up
10 to 36 photons.
11
12 **2 TESs Fabrication**
13
14 NIM fabricated TESs with two active areas (10 µm × 10 µm and 20 µm × 20
15 µm) on the wafer. Considering the reliability of the optical fiber alignment
16 and to avoid optical geometric loss. In this paper we present preliminary
17 results for the TES with 20 µm × 20 µm active area, which allows an easier
18 and better fiber optics alignment, but with a larger heat capacity that affects
19 the energy resolution. We have confirmed that the 20 µm × 20 µm Ti/Au
20 TES has sufficiently ability to resolve 1550 nm single photon detection.
21
22 2.1 Ti/Au bilayer films
23
24 The Ti/Au bilayer films are deposited on double-polished 3-inch 500 µm
25 silicon substrates with 500 nm SiN_x layers on both sides using a magnetron
26 sputtering process. The base pressure is ~10^{-6} Pa, and the sputtering pressure
27 is 0.1 Pa. Firstly, a 5 nm Ti film is sputtered as the adhesion layer. Then an
28 Au layer is deposited as the normal metal layer with a thickness d_{Au} of 60
29 nm. A variable thickness d_{Ti} of Ti layer (40 to 70 nm) is deposited on Au
30 layer.
31

Tab. 1 The ρ_{eff} and R_q of Ti/Au films

Sample	Thickness/nm		ρ_{eff}/nΩ·m	R_q/nm
	Ti	Au		
NIM-21	70	60	76	1.11
NIM-22	60	60	65	1.02
NIM-23	50	60	57	1.04
NIM-24	40	60	53	1.01

32
33   The effective resistivity $\rho_{eff,}$ root mean square roughness R_q, and T_c of the
34 Ti/Au bilayer are measured for different d_{Ti}/d_{Au} ratios. The ρ_{eff} is defined as
35 $R_\square × (d_{Au}+ d_{Ti})$, where $R_\square$ is the sheet resistance. The ρ_{eff} is proportional to

Development of an Optical Ti/Au Transition-Edge Sensor for Single Photon Detection

1 the ratio d_{Ti}/d_{Au} as shown in Tab.1. NIM-21 shows the highest ρ_{eff} = 76
2 nΩ·m, and NIM-24 shows the lowest ρ_{eff} as 53 nΩ·m, which trends to the
3 bulk Au resistivity ~ 22 nΩ·m [10]. The ρ_{eff} will be helpful for the resistance
4 design of the TESs. The R_q are similar ~ 1 nm, indicating a good interface
5 morphology between the Ti and Au layers. The smooth interface will make
6 weak proximity effect [11,12].
7   The T_c are measured in an adiabatic demagnetization refrigerator (ADR)
8 system with a base temperature ~ 30 mK and are shown in Fig.1. The weak
9 proximity effect occurs for the largest d_{Ti}/d_{Au} ratio, and the T_c of NIM-21 is
10 162 mK. Inversely, NIM-24 shows a stronger proximity effect which
11 suppresses the T_c to 72 mK.
12
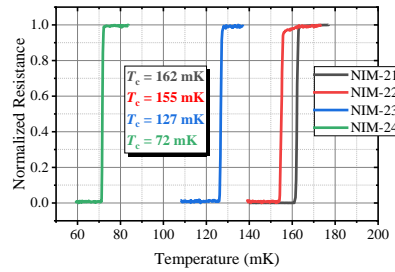
13
14 **Fig. 1** The T_c of the Ti/Au bilayers with different d_{Ti}/d_{Au} ratios. (Color figure
15 online)
16
17 2.2 Ti/Au TESs
18
19 The optical image TES device is shown in Fig. 2. The 20 µm × 20 µm active
20 Ti/Au film area is defined by UV lithography followed by a lift-off process.
21 The Nb superconducting leads for electrical wiring are also fabricated via a
22 lift-off process. The thickness of the Nb layer should be thick enough to
23 maintain its superconductivity after the following fabrication steps.
24
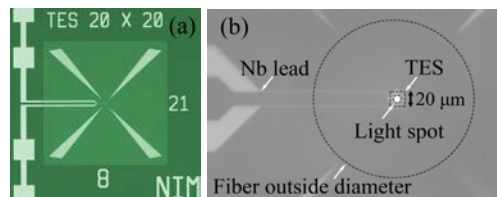

25
26 **Fig. 2** Images of an optical Ti/Au TES with a 20 µm × 20 µm sensitive area
27 with Nb leads: (a) a whole view of the TES device; (b) the enlarged view of
28 the device achieved during the optical fiber alignment process. A light spot
29 can be observed at the center of TES to locate the position of optical fiber.
30 (Color figure online)

Xiaolong Xu 1 • Mauro Rajteri 2 • Jinjin Li 1

1
2 2.3 Antireflection structure
3
4 An antireflection structure composed of SiO_2 and SiN_x dielectric layers is
5 deposited on the TES devices to reduce the device reflectivity. The vertical
6 stack structure is shown in Fig. 3(a). The SiO_2 and SiN_x layers are fabricated
7 using an inductively coupled plasma assisted plasma-enhanced chemical
8 vapor deposition (ICP-PECVD) method. The refractive index and extinction
9 coefficient (n, k) are (1.47, 0), (1.92, 0), (4.03, 3.81), (0.56, 9.91) for SiO_2,
10 SiN_x, Ti and Au at 1550 nm, respectively. These optical parameters were
11 measured using a Horiba UVISEL2 spectroscopic ellipsometers. The
12 refractive index of the UV-resin for the fiber alignment process (n = 1.56) is
13 similar to that of the fiber core (n = 1.47) [2]. With the above parameters,
14 the reflectivity at 1550 nm is simulated and shown in Fig. 3(b). The lowest
15 reflectivity is near 23%. The simulated transmittance is 10^{-3}. To control the
16 thickness accurately by the end point detection module of ICP-PECVD, 270
17 nm SiO_2 and 350 nm SiN_x are deposited on the TES device.
18
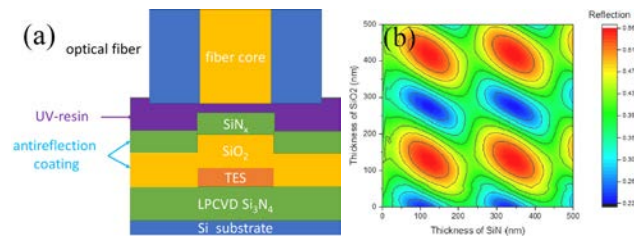
19
20 **Fig. 3** (a) the cross section of the layer structure of the TES including the
21 coupled optical fiber; (b) Simulation results of the reflectivity of the optical
22 structure. (Color figure online)
23
24 2.4 Optical fiber alignment
25
26 The optical fiber alignment process is operated with an inverted optical
27 microscope with a near-infrared CCD. The TES device is fixed on the
28 sample holder, and the optical fiber is aligned perpendicular to the device by
29 a six-dimension adjustment frame. Fig.2b shows the backside image
30 captured from the CCD. As the pig-tail optical fiber is connected to a 1550
31 nm light source, the fiber core emits a light spot. When the light spot locates
32 at the center of the TES, the resin is cured with UV light to fix the fiber to
33 the device.
34
35 **3 TES characterization**
36

Development of an Optical Ti/Au Transition-Edge Sensor for Single Photon Detection

1   The NIM-23 device shows a T_c of 95.2 mK in the voltage-biased circuit with
2   a DC-SQUID (Fig.4(a)). The TES's T_c in constant voltage mode shows
3   around 30 mK shift compared with the film shown in Fig.1. The device
4   shows a sharp superconducting transition with a width $\Delta T = 4.3$ mK. The
5   TES working point is around 6% of R_n.
6   Fig. 4(b) shows the current flowing through TES I_{TES} as a function of
7   I_{Bias} for the bath temperature T_b from 40 mK to 88 mK. The 20 mΩ shunt
8   resistance R_s on the SQUID chip is selected. From the I_{TES}-I_{Bias} curves, the
9   parasitic resistance $R_p = 10$ mΩ, the normal resistance of TES $R_n = 475$ mΩ
10 and the working point resistance of TES $R_o = 28$ mΩ at 6% of R_n can be
11 obtained. The heat capacity C of the Ti/Au bilayer is calculated as 2.2 fJ/K
12 [13].
13
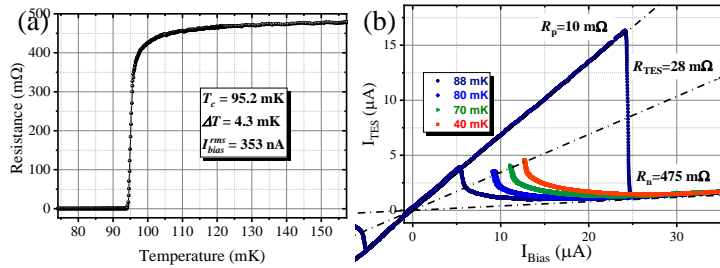
14
15 **Fig. 4** (a) The T_c of the TES device *vs.* temperature measured with a DC-
16 SQUID (b) I_{TES} *vs.* I_{Bias} at different base temperatures. (Color figure online)
17
18   The photon detection properties are characterized with a pulsed laser at
19 1550 nm. With the statistics data of the pulse signals of photons detected by
20 the TES device, the histograms of photo states are shown in Fig. 5(a) and
21 Fig. 5(b). The energy resolution ΔE is defined as the full width at half
22 maximum (FWHM) of the first photon state peak. Fig. 5(a) shows the count
23 histogram for the pulses filtered with a Wiener filter [14]. The fit of the
24 histogram with Gaussians convoluted with a Poissonian statistics (typical of
25 lasers) gives a detected mean photon number $\mu = 0.6$ photons per pulse and
26 an energy resolution $\Delta E = 0.19$ eV. In the same experimental conditions, we
27 have also continuously reduced the attenuation of the laser during the
28 acquisition, obtaining the histogram of Fig.5(b). In this case our TES can
29 clearly distinguish up to 36 photons before reaching the saturation region.
30 The typical averaged pulse response is shown in Fig. 5(c), which is fitted by
31 a double exponential equation. The electrical time constant ($\tau_{electrical}$) is
32 about 360 ns. And the response time constant (τ_{eff}) is about 107 μs.
33

Xiaolong Xu 1 • Mauro Rajteri 2 • Jinjin Li 1
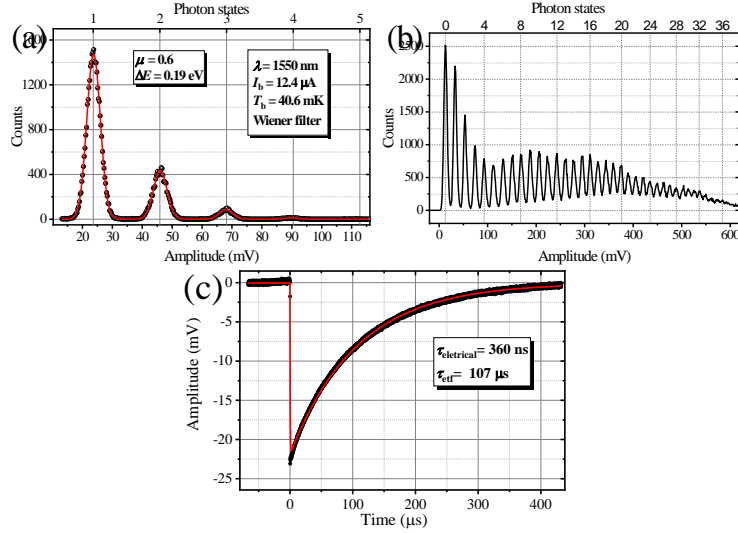
Fig. 5 Histograms of pulse height and photon states. The measurement conditions are reported in the insets. (a) The histogram is obtained from waveforms filtered with Wiener filter. The red curve is a fit with Gaussians convoluted with a Poissonian statistic; (b) The histogram is obtained directly with the signal acquired with a digital oscilloscope while the attenuation of the laser is reduced to show the whole photon states detectable with the TES; (c) Single photon pulse response. (Color figure online)

4 Conclusions

The optical Ti/Au bilayer TES device shows an energy resolution of 0.19 eV with a $20 \times 20 \ \mu m^2$ active area. The devices can discriminate up to 36 photon states. The results have shown that TESs are promising detectors for counting single photon and promote the application of TES on the optical quantum metrology. In the future, the quantum efficiency will be evaluated and improved by optimal optical cavity.

Development of an Optical Ti/Au Transition-Edge Sensor for Single Photon Detection

1   **References**

2
3   1. L. Lolli, E. Taralli, M. Rajteri, J. Low Temp. Phys. 167, 803 (2012) ,
4   DOI: 10.1007/s10909-012-0473-2
5   2. D. Fukuda et al., Opt. Express 19, 870 (2011) , DOI:
6   10.1364/OE.19.000870
7   3. A. J. Miller, S. W. Nam, J. M. Martinis, A. V. Sergienko, Appl. Phys.
8   Lett. 83, 791 (2003), DOI: 10.1063/1.1596723
9   4. R. H. Hadfield, Nat. Photonics 3, 696 (2009), DOI:
10   10.1038/nphoton.2009.230
11   5. F. Paolucci et al., J. Appl. Phys. 128, 194502 (2020), DOI:
12   10.1063/5.0021996
13   6. D. Li et al., J. Low Temp. Phys. 193, 1287 (2018), DOI: 10.1007/s10909-
14   018-2053-6
15   7. K. Nagayoshi et al., J. Low Temp. Phys. 199, 943 (2020), DOI:
16   10.1007/s10909-019-02282-8
17   8. J. R. Stevens et al., J. Low Temp. Phys. 199, 672 (2020), DOI:
18   10.1007/s10909-020-02375-9
19   9. J. C. Zwinkels, E. Ikonen, N. P. Fox, G. Ulm, and M. L. Rastello,
20   Metrologia 47, R15 (2010), DOI: 10.1088/0026-1394/47/5/R01
21   10. G. Kästle et al., Phys. Rev. B 70, 165414 (2004), DOI:
22   10.1103/PhysRevB.70.165414
23   11. K. Kengo et al., J. Low Temp. Phys. 193, 349 (2018), DOI:
24   10.1007/s10909-018-1995-z
25   12. X. Xu et al., Nanomaterials 11, 39 (2021), DOI: 10.3390/nano11010039
26   13. M. Rajteri et al., Metrologia 46, (2009), DOI: 10.1088/0026-
27   1394/46/4/S28
28   14. D. Alberto, et al., IEEE Trans. Appl. Supercond. 21, 285 (2011), DOI:
29   10.1109/TASC.2010.2087736
30